FEASIBILITY STUDY AND PROCESS DESIGN OF A DIRECT ROUTE FROM BIOETHANOL TO ETHYLENE OXIDE

Davide Ripamonti[a], Antonio Tripodi[b], Francesco Conte[a], Alessandro Robbiano[c], Gianguido Ramis[c], Ilenia Rossetti[a,b*]

a) Chemical Plants and Industrial Chemistry Group, Dipartimento di Chimica, Università degli Studi di Milano, Via Golgi 19, 20133 Milano (MI) , Italy;
b) INSTM Milano Università, Via Golgi 19, 20133 Milano (MI), Italy;
c) DICCA, Università degli Studi di Genova, via all'Opera Pia 15A, 16100 Genova, Italy

Abstract

A novel route for the direct one-pot oxidation of ethanol to ethylene oxide has been designed and scaled-up into a full process: this is the very first design of an innovative one-step conversion route from bioethanol to ethylene oxide.

Starting from the review and interpolation of reaction kinetics, a staged, cooled reactor is sized for the air-based oxidation of bioethanol, yielding ethylene oxide in one-step. An efficient strategy for the separation of the product from the gas phase effluent of the reactor is developed, based on absorption in a hydro-alcoholic solution rather than in pure water. This in turn brings a material recycle between the feed and purification section that benefits the atom economy. As the basis of an economic analysis, the energy balances are assessed and analyzed via the Pinch Analysis method. The calculations let foresee a conversion of 90% of bioethanol into Ethylene Oxide (>99% purity) and 7.7% into marketable ethylene-glycol.

Keywords: Ethylene Oxide synthesis; Bioethanol; Reaction kinetics; Reactor modelling; Distillation Column; Process simulation; Pinch Analysis.

* Corresponding author: fax +39-02-50314300; email: ilenia.rossetti@unimi.it

Introduction

Ethylene oxide is primarily used as disinfectant, sterilizing agent and fumigant when it is employed as a non-explosive mixture with N_2, CO_2, or dichlorofluoromethane. It can sterilize, for instance, surgical instruments in hospitals or to remove pests and microorganisms from spices, furs, etc. [1,2]. However, most of this product it is furtherly converted into other derivatives [3,4] (**Figure *1***).

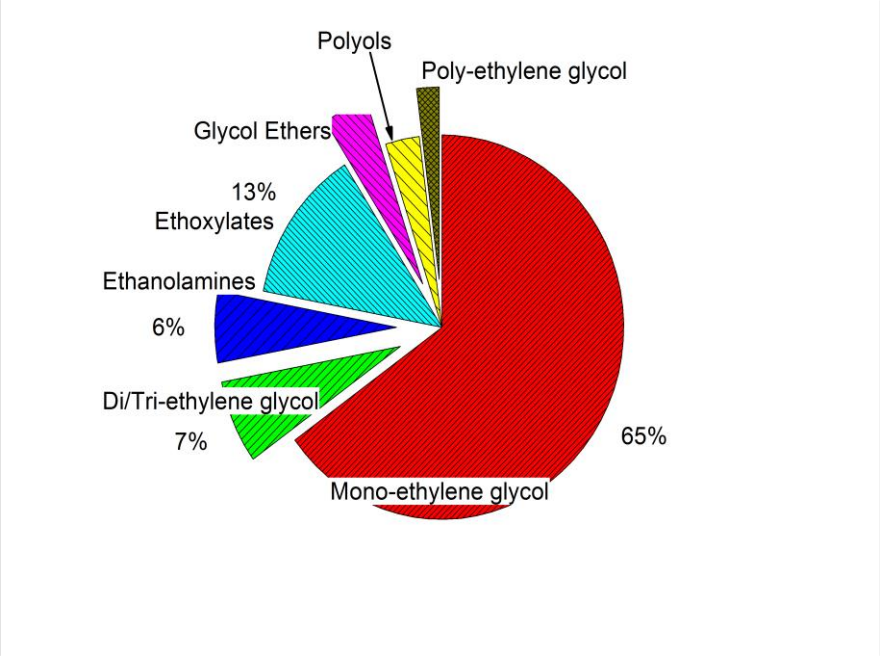

Figure 1: Ethylene Oxide derivatives. Data taken from [4].

Currently, ethylene oxide is produced by direct oxidation of ethylene with air or oxygen on supported silver catalysts; annual worldwide production capacity was ca. 1.7×10^7 tons [4], making it an important industrial chemical. Silver is deposed on a porous support material in concentrations of 7 – 20 wt% [5]. The support material is of critical importance: preference is given to ultrapure (over 99 %) aluminum oxide, in addition, 100 – 500 mg/kg of promoters such as salts of alkali and alkali-earth metals are added to improve the selectivity [5,6].

Two different processes have been implemented: the oxygen-based oxidation process and the air-based one. Shell plants use only pure oxygen [7,8], while Scientific Design and UCC have developed air-based oxidation plants as well [9]. The conversion per pass is kept low in order to control the temperature, because the reaction is highly exothermic and runaway can easily occur, so the reactor is recirculated after the first gross gas-product separation. Ethylene is converted at 200 – 300°C and 1 – 3 MPa to produce ethylene oxide, CO_2, H_2O, traces of acetaldehyde and formaldehyde [3,10]; these products must be removed or separated from the gas stream, which is then reloaded with oxygen and ethylene and returned to the reactor.

In the last decades, alternative routes to produce bulk and fine chemicals from renewable sources have been intensely studied. In particular, ethanol seems to be a promising starting reagent: in fact, this molecule has already been used to produce ethylene [11–17], acetaldehyde [18], light olefins [19,20], has been widely studied as a basis for hydrogen [21–24] with continuously optimized catalysts and processes [25–27], and has also been considered as a promising source of acetonitrile [28–30].

The indirect bioethanol-bioethylene-biooxyrane route has already been put in practice [31,32], but it needs two separate plants which, combined with the higher cost of the starting reactant in most countries, would lead to the economic unsustainability of the process. Hence, the aim of this work is to design and simulate the direct one-pot ethylene oxide production starting from bio-ethanol. The first successful experiments for such reaction have been carried out by Lippits and Nieuwenhuys [33,34], beyond other trials [35]. Results show that it is possible to selectively oxidize ethanol with O_2 on a heterogeneous catalyst directly leading to ethylene oxide through one pot reaction. Catalysts of this reaction are metals (Cu, Ag, Au) supported on γ-Al_2O_3 promoted by Li_2O and CeO_x. The reaction main interest lies in the possible simplification of the present-day bio-ethanol based process: this work explores the possibility of a one-step bioethanol-ethylene oxide production as a new and more sustainable ethylene oxide route. In particular, starting from the available literature data we have set up a kinetic model and designed the process flow diagram of a completely new production

process. Different side opportunities are also discussed for reactants recycles and the valorization of byproducts. This represents a first step for economic and lifecycle assessment of the proposed solution.

Models and Methods

a. Thermodynamic models

The mass and heat balances for the separation section of the process and the heat balance for the reactive section, have been calculated using the Aspen Plus® v10-11 software by Aspen Tech™, using the following embedded algorithms:

- Wegstein or Broyden methods for the material recycle;
- Non Random Two liquids (NRTL), UNIversal QUAsi-Chemical (UNIQUAC) and Wilson models for liquid-phase activity coefficients of condensable species (in the range 0 – 300 °C and 1 – 15 atm), choosing for each unit the best-fitting method in relation to literature data available for its specific mixture composition;
- Redlich-Kwong-Soave (RKS) equation of state for the vapor-phase fugacity coefficients;
- Henry constant for the solubility of light gases (CO_2, CO, N_2) into water in the mentioned conditions.

b. Kinetic model

The original study of Lippits et al. [34] presents a comparison between different catalysts: in this work the $Au/Li_2O/Al_2O_3$ formulation is taken as a reference, because presented the best compromise between conversion and selectivity. The reaction mechanism usually adopted for the ethylene to EO [36–40] process has been modified, in order to account for the presence of ethylene as byproduct or intermediate. From the reviewed data, it is evident that ethanol starts to convert very quickly, apparently leading directly to the formation of ethylene oxide. Then over 250 °C it starts to over-oxidise into CO_2 (and water). The ethylene formation seems to follow a different pathway, not

depending from ethylene oxide formation, likely starting from ethanol and having diethyl ether as intermediate, as already demonstrated [41,42].

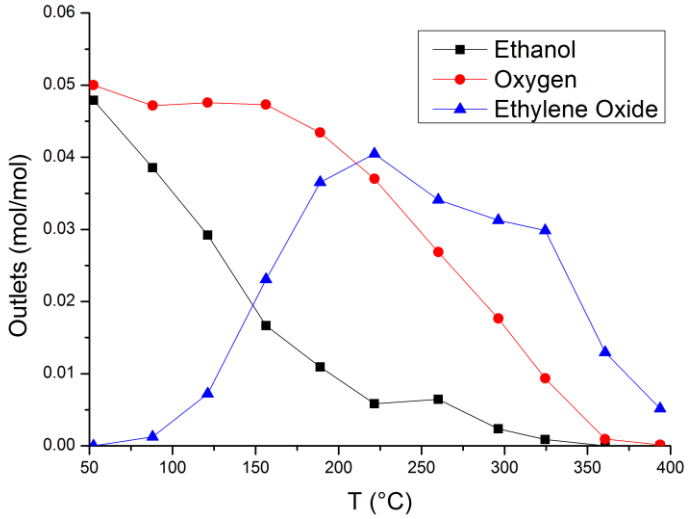

Figure 2: Ethanol (EtOH) and oxygen (O_2) and ethylene oxide (EO) mole fractions at reactor outlet as a function of reaction temperature on Au-catalysts by Lippits et al. [34] reworked from selectivity vs. conversion data.

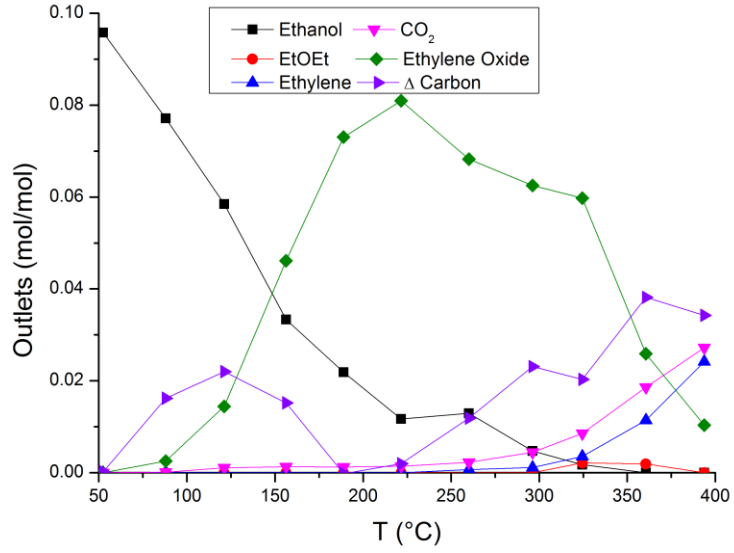

Figure 3: Products distribution and carbon balance as a function of reaction temperature, calculated from the data of Lippits et al. [34].

The published experimental results present the conversions and selectivities to the various products at different temperatures, as reported in Table S1. These have been reworked to calculate the products distribution at reactor outlet (mol) as reported in **Figure *2*** and 3. Extrapolating the carbon balance, it

is found that below and above 220°C the measured products do not account for all the converted ethanol (**Figure *3***). We hypothesise that the carbon loss below 180°C could be due to acetaldehyde formation, dominant over ethylene Oxide (EO) at lower temperatures, often masked within GC-mass analytical system because of similar retention times and equal molecular weight than ethylene oxide [35]. This intermediate is well assessed for ethanol steam-reforming reaction mechanism on similar supports. Moreover, other studies presents acetaldehyde formation from ethanol using similar catalysts and reaction conditions [24,35,43,44]. For these reasons it has been chosen to consider acetaldehyde as an intermediate, rather than a secondary product, fully accounting for the carbon missing in the experimental data. The carbon loss over 220 °C instead, can be attributed to carbon monoxide, formed when ethylene oxide combustion is not complete. Also in this case, it would not be acetaldehyde to decompose at high temperatures as in the consolidate schemes of ethylene reaction on Ag-based catalysts [40]. Taking into consideration these hypotheses, the adopted pathway is presented below (**Figure *4***).

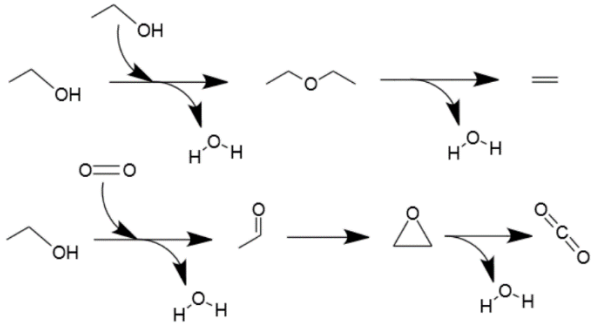

Figure 4: Adopted reaction path for the ethanol-EO conversion.

Considering this context, an original kinetic model has been drawn to fit better the data closer to 200 °C, where ethylene oxide selectivity is maximum and where the documented carbon loss is nearly zero, allowing for a higher error at higher and lower temperature, due to the problems described above.

Expressing the i-eth reaction rate as (see List of symbols for the meaning):

$$r_i = k_i \prod_j \alpha_{ij} y_j^{\nu_{ij}} \qquad (1)$$

$$k_i = k_{0i} exp\left[\frac{-E_a}{R}\left(\frac{1}{T} - \frac{1}{T_0}\right)\right] \quad (2)$$

the steady-state molar balance of a plug-flow reactor (like the one used by Lippits et al. [34] for their tests) can be written as (in terms of contact time or catalyst load):

$$\lambda \frac{\partial n_j}{\partial w} = \frac{\partial n_j}{\partial z} = \frac{\sum_i \alpha_{ij} r_i}{u} = \sum_i \alpha_{ij}\, r_i \frac{\partial \tau}{\partial z} \Rightarrow \Delta n_j = \int_0^{\tau} \left(\sum_i \alpha_{ij}\, r\right) d\tau = \int_0^{w} \left(\sum_i \alpha_{ij}\, r'\right) dw \quad (3)$$

supposing to ignore diffusive phenomena and gas-solid mass transfer resistances. This hypothesis is supported by the state-of-the-art lab-scale experiments reported in the selected literature, where very diluted gas mixtures and catalysts are used. Energy and momentum balances are neglected because the experimental apparatus used for collecting the experimental data was nearly isothermal and the pressure drop very low. Since in the reviewed tests the reactants were diluted with an inert carrier, the molar flow for each relevant compound $n_j = n_{tot} y_j$ can be approximated as: $n_j = \frac{P\dot{V}}{RT} y_j$ all along the reactor coordinate.

So for each involved species, the conversion or production Δn is a non-linear function of k_0, E_a, and w; k_0 and E_a in turn can be regressed in order to minimize the sum: $\sum_l \left(\Delta n_{calc} - \Delta n_{exp}\right)_l^2$ over all the l experiments available.

The numerical integration of equation (3) has been performed with Mathworks™ Matlab r2020® in order to obtain Δn_{calc}, and the kinetic parameters recursively adjusted to match Δn_{exp}.

c. Reactor model

The laboratory data of Lippits et al. [34] let foresee a full conversion and the higher selectivity around 220 °C. Unlike in the traditional ethylene-EO reaction, at lower conversion the acetaldehyde is markedly dominant over EO: this implies that the ethanol-EO reaction can be exploited to obtain a purer product without recycles, but only removing the full reaction heat. Indeed, if a consecutive reaction path is validated as proposed in Figure 4, operating at low temperature prevents the parallel path to diethylether and ethylene and allows a complete conversion just by managing the reaction heat to prevent runaway and, more in general, a significant increase of temperature with loss of

selectivity. This has been achieved considering three cooled reactive beds, each followed by an additional cooling stage (as represented in **Figure *5***). The number of beds is a good compromise between thermal management and cost and manageability of the solution. The selected coolant is saturated water.

The catalytic beds have been designed according to the following hypotheses:

- to increase the heat-exchange surface, the catalyst is considered packed into tubes, as typically done in shell and tube reactors, so to achieve an area:

  $$A_{ex} = \pi\, OD \times NT \times L \qquad (4)$$

- consequently, according to the catalyst loading, the tube length is:

  $$L = \frac{4\,w}{\rho_b(1-\theta)(1-\varepsilon)\,\pi\, NT \times ID} \qquad (5)$$

- for the overall heat transfer coefficient one has: $\frac{1}{h} = \frac{1}{h_{tube}} + \frac{1}{h_{tw}} + \frac{1}{h_{shell}}$, where typically $h_{tw} \geq {}^{20}/_{0.002} = 10^3 \left(\frac{W}{m^2 K}\right)$, $h_{shell} \geq 10^3$ (boiling liquid), so $\frac{1}{h} \approx \frac{1}{h_{tube}}$. For the tube-side coefficient we used the Li-Finlayson correlation [45]:

  $$h_{tube} = 2.03\,(Re^{0.8})\left(\frac{k_c}{ID}\right) e^{-\left({}^{6Dp}/_{ID}\right)} \qquad (6)$$

  valid for 20 < Re < 7600 and 0.05 < $\frac{D_p}{ID}$ <0.3, where the Reynolds number is calculated around a catalyst particle, but the fluid velocity as if the tube were empty.

- the catalyst effectiveness is calculated, for an isothermal catalyst pellet, as:

  $$\eta = \left(\frac{3}{\Phi}\right)\left(\frac{1}{\tanh \Phi} - \frac{1}{\Phi}\right) \qquad (7)$$

  other details for this calculus are found in **Errore. L'origine riferimento non è stata trovata.** in the Supporting Information file.

- the kinetic parameters are then corrected as: $k' = k \times \eta$, neglecting the lower contribution coming from the mass transfer resistance between gas bulk and solid surface;

- the reacting mixture mass balance is calculated via equation (3), while the momentum balance via the Ergun correlation:

$$\frac{\partial P}{\partial z} = \frac{(1-\varepsilon)\, u\, \rho_g}{\varepsilon^3 D_p}\left(\frac{150\, \mu\, (1-\varepsilon)}{D_p} + 1.75\, u\rho_g\right) \quad (8)$$

and the mono-dimensional steady-state energy balance, neglecting dispersions across the shell and assuming a unique temperature value for the packed tube, as:

$$\frac{\partial T_g}{\partial z} u(z) = \frac{(1-\varepsilon)\rho}{\varepsilon\, C_{pg}(z)\rho_g(z)}\left[\sum_i \Delta H_i r_i - \pi\, OD\, h\left(T_g - T_{cw}\right)\right] \quad (9)$$

$$\frac{\partial H_{cw}}{\partial z}\left[\frac{4\, F_{cw}}{\pi\left(D_{shell}^2 - NT \times OD^2\right)\rho_{cw}(z)}\right] = \pi\, NT \times OD\, h\left(T_g - T_{cw}\right) \quad (10)$$

$$\begin{cases} \frac{\partial T_{cw}}{\partial z} = \frac{1}{C_{pcw}}\frac{\partial H_{cw}}{\partial z} & T_{cw} < T_{sat} \\ \frac{\partial x_{cw}}{\partial z} = -\frac{1}{\Delta_{ev}H}\frac{\partial H_{cw}}{\partial z} & T_{cw} = T_{sat} \\ \frac{\partial T_{cw}}{\partial z} = \frac{1}{C_{psteam}}\frac{\partial H_{cw}}{\partial z} & T_{cw} > T_{sat} \end{cases} \quad (11)$$

To simulate the actual reactor, eq. (3) is not solved independently at constant temperature and pressure any more, but is integrated together with equations (8) and (9), directly within the Aspen Plus flowsheet.

Since the above mentioned calculations requires some results as input data, the following procedure has been followed. This time, the Aspen Plus 'PFR' block unit was used in some passages, because this software has got extensive thermodynamic libraries to calculate automatically reaction enthalpies and other relevant properties (density, viscosity, etc.):

1. the number of tubes, the diameter and catalyst loading are chosen;
2. the tube length is calculated according to relation (5), provided that $L \geq 10\ OD$;
3. a large excess of saturated water is used as coolant;
4. η for reactions 1-3 is calculated at the bed inlet conditions, save for the temperature which is set at $T_{g,in} + 25$, and the kinetic constants corrected;
5. equations (3) and (8) – (11) are solved by the Aspen Plus PFR integrator, after having provided the heat transfer coefficient through equation (6);
6. the following conditions are then checked:

a. the exit temperature must not exceed the inlet one by more than 50°C,
b. the stage conversion must be higher than 20%,
c. the pressure drop must be acceptable ($\leq$ 1 bar for the whole reactor, given the low pressure adopted);

if needed, the procedure is repeated updating the values assumed in step 1 (also the catalyst particle size is allowed to vary slightly, provided that $ID \geq 10D_p$, and the saturated coolant pressure is modified in the range 4-10 bar).

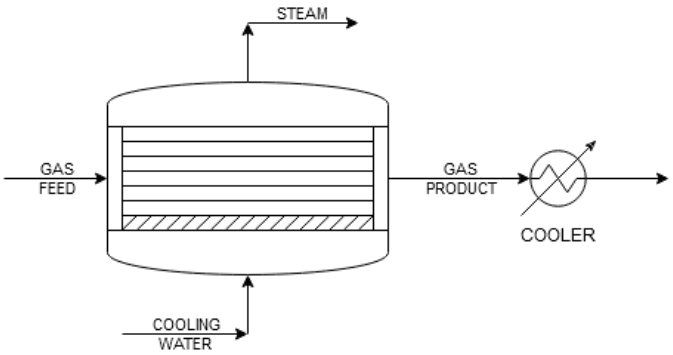

Figure 5: Scheme of a single reaction stage, of the three in series.

d. Separation section

The purification section carries out several tasks connected to each other:

- since renewable bio-ethanol is supposed to be the feedstock, it must be purified from water;
- the produced EO must be liquefied and separated from N_2 and CO_2, acetaldehyde is eventually removed in a dedicated column;
- since we separate EO from the gas through a washing, before the final purification an additional stripping unit is needed, accounting then for a minimum of 4 separation units (see Figure *6*).

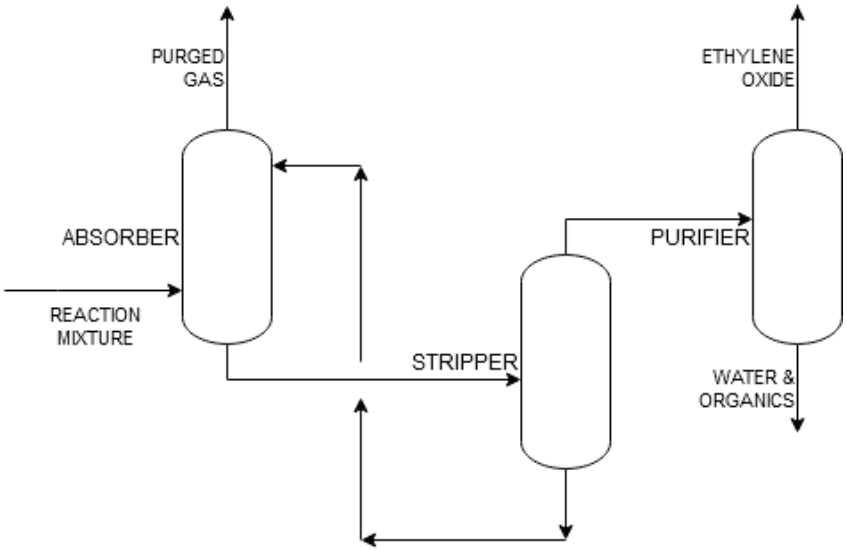

Figure 6: Basic layout of the purification section.

This scheme has been furtherly expanded considering three aspects:

- EO-acetaldehyde purification leaves some product in the bottoms: this already reacts with water to yield ethylene-glycol [46] and even more efficiently through specific catalysts [47];
- this latter compound can be used as entrainer in the ethanol-water azeotrope separation to reduce the column equivalent trays thanks to the induced volatility enhancement (in our case it is not needed to resolve the azeotrope, even if this technique would make it possible) [48];
- EO washing from the reaction gases is more effective if a hydro-alcoholic mixture is used instead of pure water [49].

According to these reasoning, the ethanol-feeding section and the EO washing-stripping modules become tightly connected. The ethanol concentration section is furtherly divided into two blocks, because the initial water content of a fermented beer is so large – and the absorber requirements relatively different from the reactor ones – that different internal setups become necessary.

The entrainer leaving the ethanol purifier in the bottoms is recycled in a glycol-water separation column that receives also the product of a dedicated column that accomplished the catalytic conversion of waste EO into Ethylene Glycol. This solution (**Figure *7***) presents the following characteristics:

- advantages: i) no EO is wasted (since the amount that cannot be separated form water and acetaldehyde becomes ethylene-glycol, fully separable from such a mixture), ii) more efficient feeding ethanol concentrator and absorber are designed;
- issues: two more operation units are needed, and the recycle layout becomes more complex.

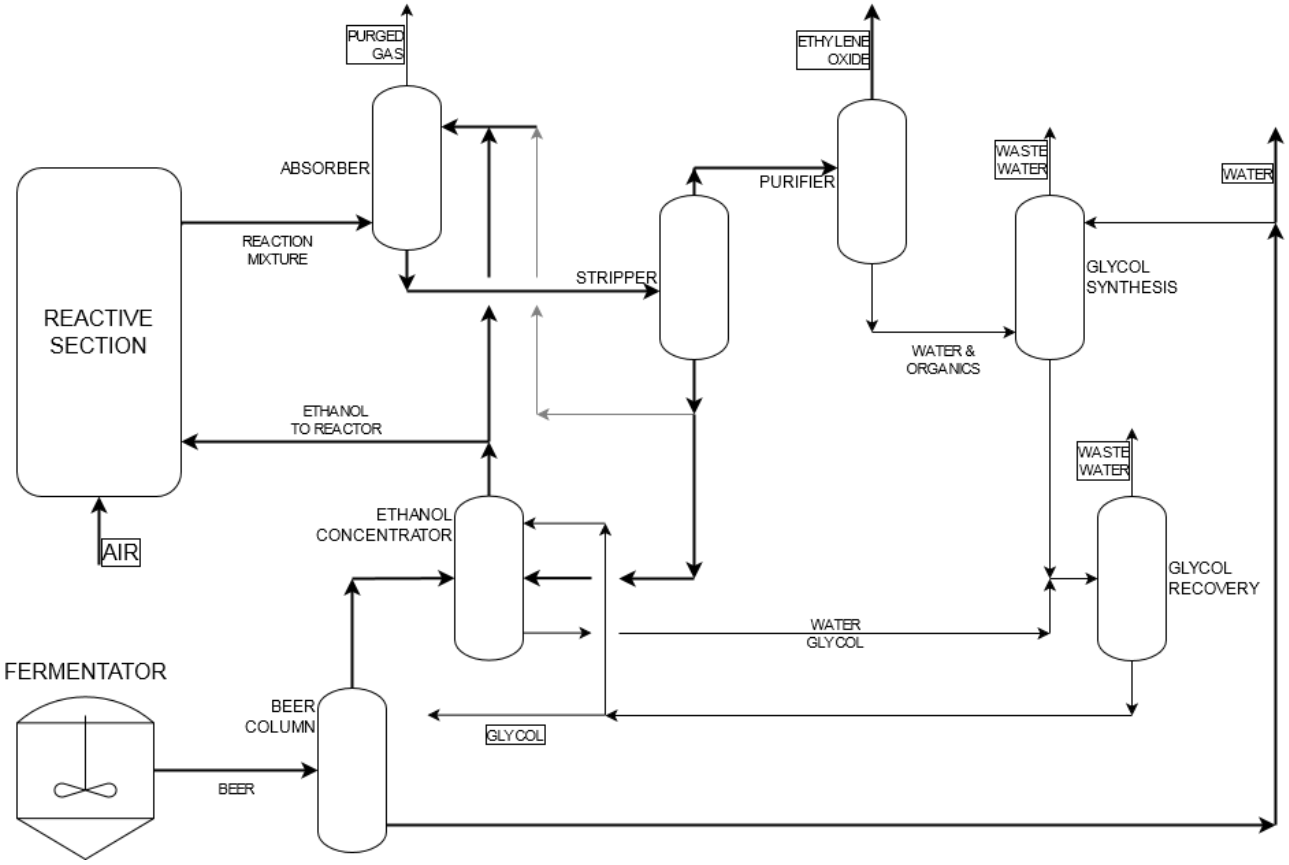

Figure 7: Final layout of the purification section.

The detailed sizing of the seven separation blocks and the solution of the mass recycles has also been carried out with Aspen Plus, since this software is particularly well suited for the distillation design. The recycle convergence requires some extra care, especially for the presence non-condensable species that can build up if the absorber calculation deviates from the design target.

The procedure to size the distillation columns is as flows:

1. the VLE properties of the main mixture components were reviewed [50–57] and the best-fitting thermodynamic model chosen;
2. the column internals are chosen according to plant data or references available;

3. the correlations used for mass transfer, interfacial area, and liquid holdup (when reactions are involved) are directly available within the Aspen Plus package, so this complex part of the calculations does not need to be worked up separately; the selection used by the software is:

Column type	**Mass transfer**	**Interfacial area**	**Liquid holdup**
Packing	Bravo et al.	Bravo et al.	Bravo et al.
(absorber)	Onda et al.	Onda et al.	
Sieve trays	Chan and Fair	Zuiderweg	Bravo et al.
Valve trays	Schaffe and Weiland	Schaffe and Weiland	

The heat transfer between the phases is always estimated through the Chilton-Colburn method, according to Taylor & Krishna [58]. The pressure drops are computed by semi-empirical correlations provided by the packing vendors, or by the Smith's method [59] for trays.

The flooding criterion is always set to 80 % of maximum vapor velocity [60]; the liquid and vapor compositions are considered constant on each stage (theoretical or actual), while the double-layer resistance between the gas and liquid bulk phases is considered.

The essential characteristics of the columns are reported hereafter in **Table *1***, while the supporting material can be browsed for the full VLE consistency assessment.

Block	**Top Pres**	**Column Internals**	**Stages height**	**Bottoms: feed**	**Reflux ratio**	**Product Recovery**	**Product Purity**	**General Reference**
	(atm)		(m)	(mol/mol)	(mol/mol)	(%)	(mol %)	
PURIFIER	1.3	Sieve trays	40	0.0677	4.7	94.3	99.5	[61]
GLYCOL SYNTHESIS	4.4	Mellapak	10.0	0.48	7.0	95.3	16.3	[62]
BEER COLUMN	0.10	Flexipac Flex-trays	5.07	0.98	2.5	99.5	70.6	[63]
GLYCOL RECOVERY	1.0	Durapack	3.6	0.29	0.2	98.9	90.8	[56]

ETHANOL COLUMN	1.1	Mellapak	3.6	0.60	0.19	98.6	90.2	[55][64]
ABSORBER	5.0	Raschig	4.0	0.72	-	99. 9	0.0649	[49]
STRIPPER	2.0	Mellapak Sieve trays	8.0 14	0.93	1.8	96.2	98.1	[65]

Table 1: Columns specifications. In the case of the absorber, the bottoms:feed ratio is the one obtained, not imposed. The recovery of the glycol synthesis column represents the conversion of the reaction EO → glycol.

The absorber design has required a dedicated procedure, because this block has been validated against available experimental data [49] as follows:

1. the equilibrium single-stage separation for the mixture: EO, N_2, water, ethanol has been evaluated by the VLE model at different mixture composition and an average $m = {y^*}/{x^*}$ value for EO in the hydro-alcoholic mixture has been obtained;
2. a test column has been set up in Aspen Plus following as close as possible the characteristics of the laboratory apparatus described by Bonilla et al. [49], save for the gas flow rate (fixed at 1 kmol/h) and the liquid flow rate (variable);
3. applying the formulas for the packing height (z), equivalent transfer units height (HTU_{OG}) and theoretical packing units number (N):

$$z = N \times HTU_{OG} \tag{12}$$

$$HTU_{OG} = HTU_G + HTU_L \frac{mF_G}{F_L(1-y_{top})} \tag{13}$$

$$N = \frac{2.3}{1-\frac{mF_G}{F_L}} ln\left[\left(1-\frac{mF_G}{F_L}\right)\frac{y_{bot}}{y_{top}} + \frac{mF_G}{F_L}\right] \tag{14}$$

and retrieving the simulation results (imposing z, F_G and F_L the software yields y_{top} and y_{bot}), one can calculate all the relevant quantities. The cases compliant with the available experimental results [49] have been furtherly refined selecting only those F_L – F_G couples which yielded feasible hydraulic conditions in the column;

4. with HTU_{OG} and $\frac{mF_G}{F_L(1-y_{top})}$ showing a linear trend between themselves, HTU_G and HTU_L can be regressed, then the last two steps are repeated correcting the interfacial area (calculated automatically by Aspen Plus) by a factor <1 [66], until the values of 0.37 and 1.71 are found (with respect to the experimental values of 0.32 and 1.82 [49]) for an effective area equal to 80% of the theoretical one.

The connection of the reactive and purification sections in a larger Aspen Plus flowsheet has required further adjustments in the ethanol concentrator (to grant a feed of the correct composition) and, in turn, in the reactors internals (to grant in return a product mixture of the foreseen composition).

The plant size has been decided according to an average bioethanol fermenter capacity of 75 m^3/h of beer [3], meaning 120 – 130 kmol/h of ethanol available to feed the reactor.

e. Heat balances

The total energy input and output of the process have been calculated using the Pinch Analysis technique as exemplified in the practical guide by Kemp [67].

The hot and cold streams have been considered with and without the auxiliary steam circuit foreseen to cool the reactor and four different values of a global ΔT_{min} have been investigated: this first analysis has been conducted on Matlab with a customized script (the same software has been used to print the Stream Charts), in this case the total exchange area foreseen to meet the energy targets has been evaluated as: $A = \frac{Q_{in}-Q_{HU}}{U\ \Delta T_{min}}$

Where Q_{in} is the total heat required by the cold currents, Q_{HU} the hot utility target and *U* the average heat exchange coefficient representative of the whole process, set to 500 W/m^2 °C. Then another analysis has been run on the overall fluid list (*i.e.* process currents plus steam) introducing customized ΔT_{min} values for each stream, according to the following guidelines:

- ΔT_{min} = 10 °C for liquids;
- ΔT_{min} = 15 °C for vapors;

- ΔT_{min} = 5 °C for condensing vapors or boiling liquids;

In this case the analysis has been run using Aspen Tech Energy Analyzer: this tool has also been used to design the stream couplings, in order to foresee the number and duty of the regenerative heat exchangers without encumbering the Aspen Plus flowsheet with more than 20 additional blocks, each with a nested recursive calculation.

Results

a. Reaction kinetics

The result of the kinetic analysis and quantitative reassessment of the experimental results are presented synthetically in **Table *2*** and documented more extensively through **Errore. L'origine riferimento non è stata trovata.**, **Errore. L'origine riferimento non è stata trovata.** and **Errore. L'origine riferimento non è stata trovata.** in the Electronic Supplementary Information file.

The activation energies follow essentially the selectivity peaks of the reviewed data [34].

Reaction	Stoichiometry	Rate $\left(\frac{mol}{s \times kg_{cat}}\right)$	k_0 $\left(\frac{mol}{s \times kg_{cat}}\right)$	E_a $\left(\frac{kJ}{mol}\right)$
1	$C_2H_6O + \frac{1}{2}O_2 \rightarrow CH_3CHO + H_2O$	$r_1 = k_1\, y_{C_2H_6O} y_{O_2}^{1/2}$	12.00	33
2	$CH_3CHO \rightarrow (CH_2)_2O$	$r_2 = k_2\, y_{CH_3CHO}$	1.7	45
3	$(CH_2)_2O + 2O_2 \rightarrow CO + CO_2 + 2H_2O$	$r_3 = k_3\, y_{(CH_2)_2O} y_{O_2}^2$	0.30	85
4	$2C_2H_6O \rightarrow C_4H_{10}O + H_2O$	$r_4 = k_4\, y_{C_2H_6O}$	4.0×10^{-4}	145
5	$C_4H_{10}O \rightarrow 2C_2H_4 + H_2O$	$r_5 = k_5\, y_{C_4H_{10}O}$	7.0×10^{-5}	190

Table 2: Reactions with their regressed Arrhenius parameters. T_0 was always fixed at 220 °C.

b. Reactive stages

The simulated composition and temperature of the reaction mixture through the catalytic tube is represented in **Figure *8*** and **Figure *9***, for the data of **Errore. L'origine riferimento non è stata trovata.**. The first and second stages are very sensitive to the catalyst load and coolant temperature, because of the high fraction of fresh reactant, while the third stage needs a much higher catalyst load

to achieve the complete conversion, but keeps producing heat due to the increasingly important role assigned to EO parasitic combustion.

Actually, the last stage is designed to eliminate the need of a recycle (and its relative purge), not to contribute significantly to the EO overall yield: this choice seems all the more appealing as the oxidation process is carried out with air rather than pure oxygen.

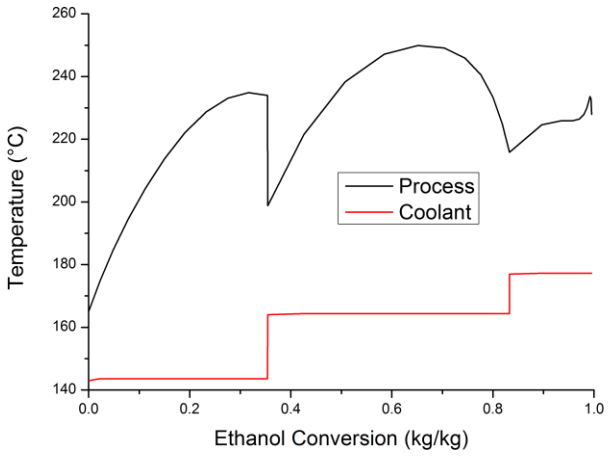

Figure 8: Reactors temperature vs. ethanol conversion.

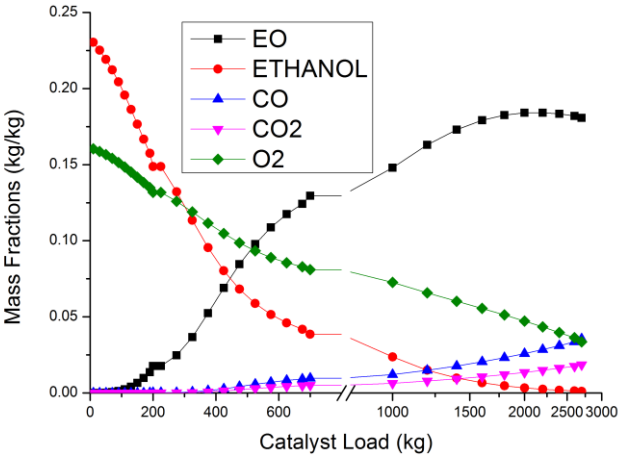

Figure 9: Evolution of the molar fraction of various species across the reactors.

c. Purification unit operations

The results calculated for the units of the purification section are presented for each block separately.

Absorber

The first design step, i.e. the evaluation of the equilibrium partition between EO and water, has yielded the results reported in **Errore. L'origine riferimento non è stata trovata.** and Figure S4. Then the test-absorber simulation results, reviewed in light of eq. (12-14), yielded the N and HTU values reported in **Errore. L'origine riferimento non è stata trovata.**.

Liquid and vapor flows are then manipulated (maintaining their ratio within the validated range) in order to obtain a feasible hydraulic column behavior, which leads to the following restricted set of options (**Table**):

F_L	$\frac{mF_G}{F_L(1-y_{top})}$	y_{top}	N	HTU_{OG}
(kmol/h)	**(mol/mol)**	**(mol/mol)**		**(m)**
0.30	0.43	0.052	2.21	1.15
0.34	0.38	0.048	2.39	1.06
0.37	0.35	0.046	2.52	1.01
0.40	0.32	0.043	2.65	0.959
0.45	0.29	0.040	2.85	0.893

Table 3: List of the feasible F_L operative range; F_G is fixed at 0.08 kmol/h.

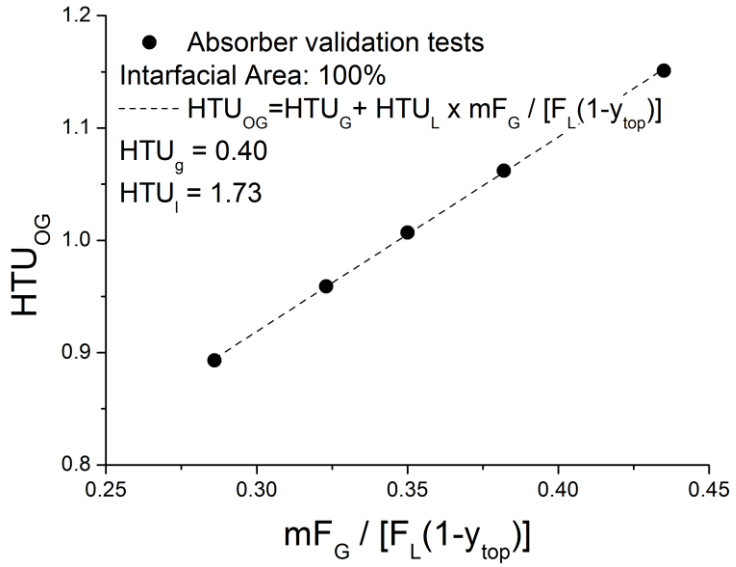

Figure 10: First fit of HTUG and HTUL following the model validation procedure of the absorber.

On this basis, HTU_G and HTU_L can be fitted (see also **Figure *10***). The discrepancy between the simulated and experimental value has been reduced decreasing the interface area actually available to accomplish the vapor-liquid mass transfer; setting it to the 80% of the theoretical value, a compromise is found with HTU_G =0.37 and HTU_L =1.71 (instead of 0.32 and 1.82).

The essential parameter to keep low the EO loss is the absorber pressure, set to 5 atm (see **Figure *11***),

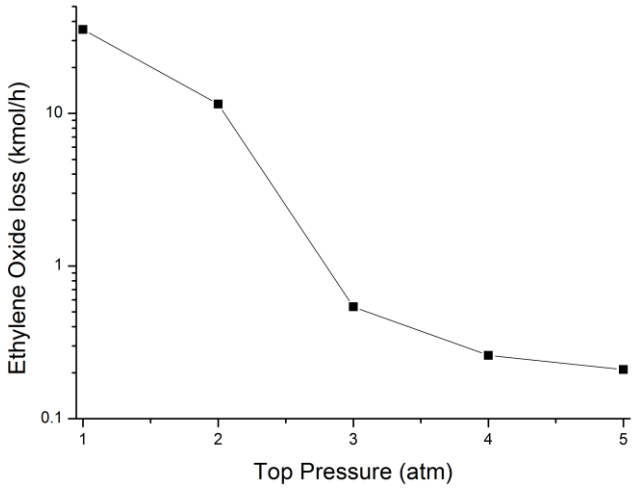

Figure 11: Study of the EO recovery as a function of absorber top pressure.

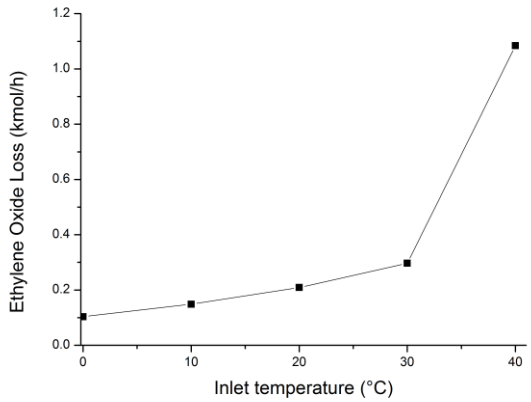

Figure 12: Study of the EO recovery as a function of absorber inlet temperature.

On the contrary, the temperature effect was not so important below 30 °C (**Figure *12*-Errore. L'origine riferimento non è stata trovata.**). The solvent is an equimolar mixture of water and ethanol, with a flowrate of 1200 kmol/h (L/G=1.15); the packing height is progressively reduced,

starting from a very large value, until the column performance (with everything else equal) is seen to reduce, and the diameter is calculated accordingly. The column recovers 99.9% of EO.

Stripper

This block relies on the same thermodynamic assessment already performed for the absorber, but no experimental data were reviewed to perform a thorough model validation, so the correlations automatically chosen by the software have been used with their default parameters.

To refine the calculation, the un-catalyzed EO hydration to ethylene-glycol has been taken into account, according to the work of Melhem et al. [46].

The first design problem solved for this unit is the trade-off between the condenser pressure and temperature: a high pressure makes more EO remain in the reflux, but increases the cooling utility temperature (see **Figure**), hence the adopted value of 2 atm revealed a good compromise.

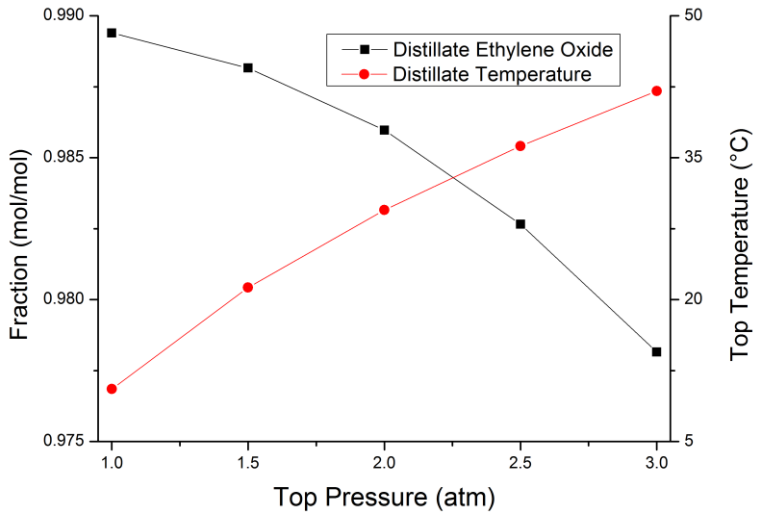

Figure 13: Stripper performance according to its chosen top pressure.

Starting to simulate a simple equilibrium-trays column, two opposite hydraulic behaviors are detected below and above the feed tray, with F_L/F_G equal to 6 and 0.5 respectively: this finding has led to

design two different column sections, recognizable also in the different pressure drop characteristic (**Errore. L'origine riferimento non è stata trovata.**).

Furtherly adjusting the try number and reflux ratio, the values of 98% purity and recovery have been calculated.

Ethylene oxide purifier

The task of this unit is essentially to retrieve as much EO as possible in the distillate, without acetaldehyde: a high number of stages is needed, as anticipated by the VLE equilibria in **Errore. L'origine riferimento non è stata trovata.** and S8. The feeding stage divides the tower in zones with different F_L/F_G ratios (**Errore. L'origine riferimento non è stata trovata.**), but in this case the range (0.8 – 1) is not very large and a single column diameter is feasible.

As in this block there is the narrowest volatility difference between the key species, the tower is the highest and is quite sensitive to the type of internals, as shown in **Table 4**.

Packing / tray type	Number of trays – packed height	Pressure drop
Mellapak 250Y	25 m	0.06 atm
Sieve	48 trays – 29 m	0.38 atm
Bubblecap	48 trays – 29 m	0.77 atm
Valve	48 trays – 29 m	0.5 atm

Table 4: EO purifier packing comparison; EO purity fixed at 99.7% wt.

In this case, assuming a tray spacing of 0.61 m, trayed columns are taller and with higher pressure drops respect to a packed one, yet the sieve trays have been chosen as a good compromise between performance and cost. The tower final simulation (with 40 trays) can recover 94% of the produced EO, keeping acetaldehyde within the limit of 100 ppm (**Errore. L'origine riferimento non è stata trovata.**).

Glycol unit

As anticipated, this block converts into Ethylene Glycol (EG) the unrecovered EO, so this strategy may be subjected to further cost-optimization assessments, as a second purifier (or even to allow a loss of the product) may be less expensive. This recovery strategy is suggested by the fact that the EO-EG conversion is anyway ongoing in aqueous solution, and it can be accelerated by a catalyst.

In this case a packed tower has been considered, additionally loaded with the active material Amberjet 4200™, suggested by the work of Altiokka and Akyalçin [68].

For this block, the thermodynamic assessment has suggested the Wilson model as the best compromise for a correct description of phases behaviour (**Errore. L'origine riferimento non è stata trovata.**). Then the general conditions of the experimental reference [68] have been followed (3.4 bar, H_2O:EO=5:1 mol/mol) in order to keep the kinetic model within its validation ranges.

Since the Aspen Plus built-in reactive rates (for distillation columns) are calculated taking the liquid holdup as basis, the reference kinetic constants are valid only supposing to load as much catalyst as to equal the reference anions concentration (0.15 mol/L) within the liquid.

As confirmed by a case-by-case analysis (**Errore. L'origine riferimento non è stata trovata.**), the best feeding stages are to the top for the fresh water and to the bottoms for the EO-water mixture exiting the purifier, while the reflux ratio has a minor importance with respect to the packing height (**Errore. L'origine riferimento non è stata trovata.**).

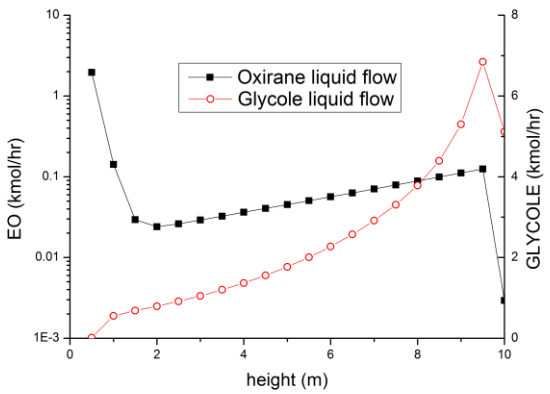

Figure 14: Liquid molar flowrates in the glycol recovery unit.

This unit can convert and recover 95% of the EO (otherwise lost) as EG, diluted to 40 % wt in water (Figure 14).

Glycol-water separator

This block's calculation has been compared with the pilot-scale work of Zaboon et al. [56]. After specifying within Aspen Plus a column as that described in the reference paper, the simulation of 4 test-cases (**Table 5**) has shown that the default calculation parameters were fully capable to represent the system.

Case	Reboiler T (°C)	Reflux Ratio (mol/mol)	Ethylene Glycol (g/g) experimental	(g/g) simulated	Error (g/g)
1	130	0.44	0.776	0.774	0.26
2	135	0.52	0.834	0.834	0.00
3	137	0.52	0.848	0.849	0.12
4	140	0.44	0.864	0.861	0.34

Table 5: Aspen Plus model validation for the glycol recovery unit.

Coming to the detailed design, a variable diameter has been foreseen, in order to accommodate the higher liquid flowrate toward the bottom (the vapor flowrate being nearly constant, **Errore. L'origine riferimento non è stata trovata.**S14) without increasing the pressure drop, also considering the increasing viscosity of the fluid in the lower stages following the glycol concentration (**Errore. L'origine riferimento non è stata trovata.**).

Beer concentrator

A pretreatment of the raw hydro-alcoholic feed was necessary for the following reasons:

- typical fermentation processes yield ethanol concentration ca. 10 vol%, or however below 20 vol% [63], much less of what is recycled from the absorber-stripper couple;
- eliminating part of the water, less glycol is needed to furtherly enhance ethanol purity imagining to set this plant into an integrated biorefinery. Indeed, for this process there is no

need to use anhydrous ethanol, but in general, glycol can be effectively used as entrainer for its purification. Thus, one of the products of this process can be used to upgrade part of the fermenter output dedicated to other uses.

This unit has been sized to achieve a purity of 70 mol% and it is designed with the condenser at 10 kPa (**Figure**) and the reboiler at 36 kPa: although this choice may be subject to further economic assessment, it has proven beneficial in terms of energy recoveries (see the section Energy Analysis).

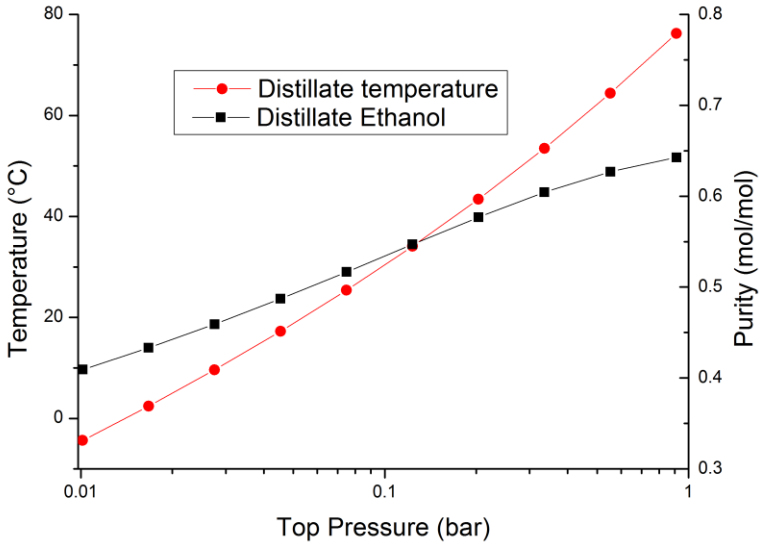

Figure 15: Ethanol purity form a 10-stages test equilibrium column, fed in the middle and yielding 1.4 moles of distillate per mole of fed ethanol, according to different condenser pressures.

Test runs with an equilibrium model have suggested a feed stage in the middle, while the reflux ratio and the number of trays saturates the block performance above 2.2 mol/mol and 14 respectively (this reflects the thermodynamic constraint due to the azeotrope, **Figure 16**).

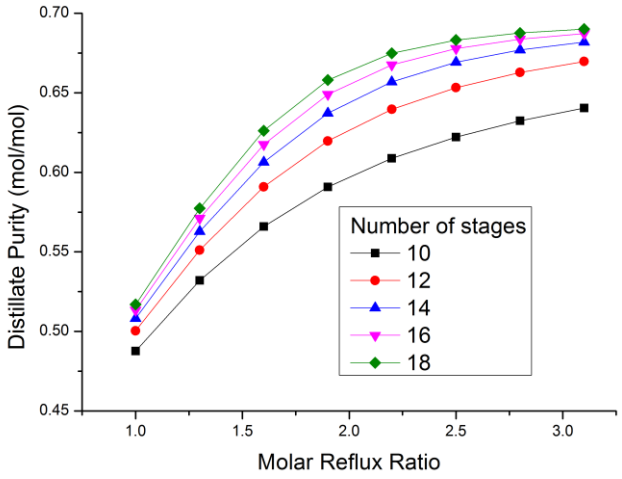

Figure 16: Test analysis of the beer column, performed with an equilibrium-stages model.

In this case, the big difference in liquid flow above and below the feed (**Errore. L'origine riferimento non è stata trovata.**) has been dealt with designing two different column internals (Flexipac HC® packing for the rectification section, Superflux® valve trays for the stripping one) for a unique diameter, considering the specific constructive and operative provisions by Koch-Glitsch for this mixture [69]. The results are synthetically displayed in **Errore. L'origine riferimento non è stata trovata.**.

Ethanol concentrator

This unit is essential in the flowsheet arrangement, because it accomplishes three tasks: i) it concentrates the beer, ii) it recovers the ethanol used as EO absorption solvent in the absorber, and iii) integrates the glycol cycle with the reactor-feeding section. The effect of EG on the ethanol-water VLE has been described following the previsions of Roja et al. [55], who used the UNIFAC (UNIQUAC Functional-group Activity Coefficients) model (**Errore. L'origine riferimento non è stata trovata.**).

A preliminary calculation on an equilibrium column has shown that the entrainer has to be fed together with the reflux, while the hydro-alcoholic feed (ethanol:water=1:1 mol/mol) can be fed

towards the column middle; two packed sections accommodate the appreciably different liquid flow above and below the feed (**Errore. L'origine riferimento non è stata trovata.**).

After setting up the column to be calculated with rate-based methods, the flow of glycol has been optimized to yield slightly over-azeotropic ethanol with a very compact unit (height 3.6 m, diameter 1.5 m); the liquid composition along the block is shown in **Figure 17**.

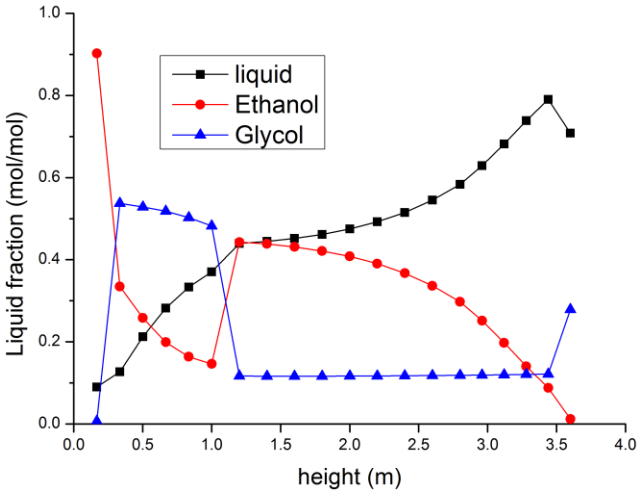

Figure 17: Concentration profile along the ethanol concentrator.

d. Energy Analysis

The complete fluid list, with the Stream Chart and Heat Exchangers Network are found in the Supporting Information, Table S6. The overall heat balances of the system are reported in **Table** and **Table** . The case with a global ΔT_{min} of 7 °C is very close to the case when specific ΔT_{min} values are applied to each streams, because the greatest contribution to the duties comes from the column condensers and reboilers, together with the boiling water in the reactor, for which ΔT_{min}= 5 °C has been set.

Process Streams Balance

Case	ΔT_{min} (°C)	T_{pinch} (°C)	Hot Utility (kW)	Cold Utility (kW)	Recoverable Heat (kW)
A1	20	82.0	16435	24245	15572
A2	15	79.5	15700	23510	16307

A3	10	77.0	13282	21092	18725
A4	7	75.5	11182	18992	20825

Table 6: Energy balance and targets for the process streams only. Total Heat Input: 32010 kW, total Heat Output: 39820 kW.

Process Streams and Water-Steam Balance

Case	**ΔT_{min} (°C)**	**T_{pinch} (°C)**	**Hot Utility (kW)**	**Cold Utility (kW)**	**Recoverable Heat (kW)**
B1	20	82.0	16450	24245	21860
B2	15	79.5	15710	23510	22600
B3	10	77.0	13300	21092	25010
B4	7	75.5	11200	18992	27110
B5	local	74.5	11270	19064	27050

Table 7: Energy balance and targets for the process streams plus the reactor cooling water. Total Heat Input: 38310 kW, total Heat Output: 46110 kW.

Referring to the overall process cases, **Errore. L'origine riferimento non è stata trovata.** reports the expected trends of the cumulative utilities target and the foreseen area for the regenerative heat exchangers: the step around $\Delta T_{min} = 10\,°C$ is due to two major hot and cold streams that could be crossed for $\Delta T_{min} \leq 9$ °C but cannot if $\Delta T_{min} \geq 11$ °C, i.e. the reboiler of the beer concentrator and the condenser of the ethanol concentrator (see also **Errore. L'origine riferimento non è stata trovata.**).

Referring to cases ‘A4’ and ‘B4’ (**Table** and **Table**), which yield targets very similar to the less approximate calculation with multiple ΔT_{min}, **Figure** shows the positions of the reactor cooling circuits in the process temperature range. Since this utility is designed as a closed circuit, its inclusion within the PA does not alter the hot and cold utilities targets with respect to the base case: moreover, the lowest foreseen pressure for the steam-raising is 4 bar (for the first reactor bed), so supposing to maintain the whole circuit at this pressure the rejected heat is kept 50 °C above the pinch, and it can conveniently be transferred to a cold stream rather than to a heat sink.

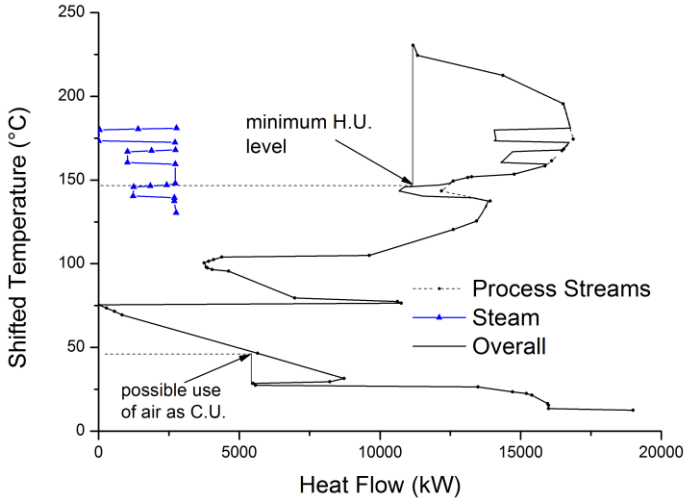

Figure 18: Grand Composite Curve (GCC) for the process streams and the process streams plus the reactor cooling.

The foreseen regenerative heat exchangers are listed in **Errore. L'origine riferimento non è stata trovata.** and can be found in **Figure** . The unit 'E115' could carry out the crossing between the reboiling beer and one of the other columns condensate that is essential to shift the utility figure to the left side of **Errore. L'origine riferimento non è stata trovata.**: this result can be achieved adopting a vacuum column for the first ethanol concentration.

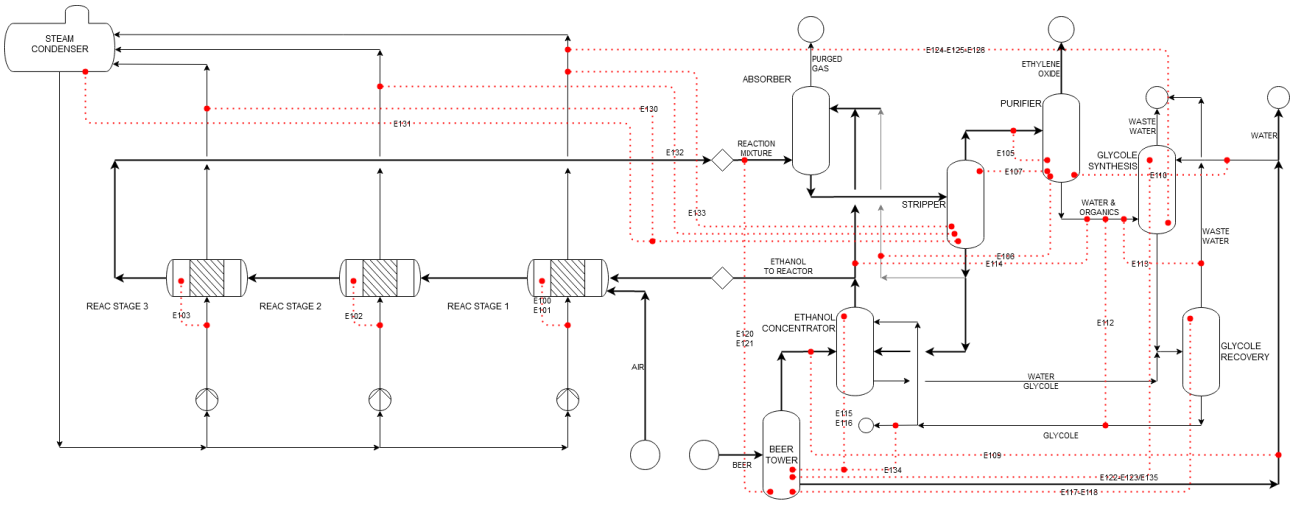

Figure 19: General process flow diagram, with the regenerative heat flows highlighted via dotted lines.

An examination of the Grand Composite Curve (GCC, **Figure**) suggests that at least a quarter of the discharged heat can be removed not below 50 °C, making it possible to use air; while providing heat

at the lowest theoretical level (150 °C) may be unpractical if the raised steam is coupled with the columns reboilers. Anyway, heating up the feed with an external source would not require a utility hotter than 180-200 °C, which makes this process suitable to play the role of a 'bottoming cycle' for larger waste-heat producers.

This first analysis solves the problem of satisfying all the cold streams below the pinch, but leaves some unsatisfied hot streams above the pinch (Figures S20 and S21): however the final assessment between the addition of other recovery units or the energy penalty due to misplaced heat sinks can be done only after the utilities are definitely selected, in order to evaluate properly the exchange area.

At last, some of the key features of the process are summarized in Table 8.

Separation section		Reactive section	
Ethylene oxide purity (mass %)	99.72	Feed temperature (°C)	165.0
Pure EO flowrate (kmol/h)	89.57	PFR-1 outlet temperature (°C)	239.0
Acetaldehyde content in EO (ppm)	29	PFR-2 inlet temperature (°C)	202.0
Water content in EO (mass %)	0.10	PFR-3 inlet temperature (°C)	216.9
Ethylene glycol purity (mass %)	99.99	PFR-3 outlet temperature (°C)	202.9
Pure glycol flowrate (kmol/h)	7.95	Coolant pressure PFR-1 (bar)	4.0
Ethanol in extractor distillate (mol %)	90.12	Coolant pressure PFR-2 (bar)	7.0
Ethylene oxide loss (kmol/h)	2.70	Coolant pressure PFR-3 (bar)	9.4
Ethanol loss (kmol/h)	8.64	Feed pressure (bar)	15.0
		Product pressure (bar)	13.1

Table 8: Selected features of the process.

This study throws the basis for the next economic assessment step, thus the detailed cost analysis is not yet available. However, at least a preliminary overlook to the most expensive items can be given. The basis is the heat integrated flowsheet, that strongly limits the utilities supply needs.

As for the operating costs, one of the highest duties is the one of the air compressor to operate the reactor at 15 bar (ca. 2.4 MW). Nevertheless, heat recovery in the reactor allows a consistent production of steam that can be used in steam turbines to supply at least part of the electric energy needs (-0.32, -1.7 and -2.3 MW partially recoverable for the three reactor stages).

As a very preliminary analysis, capital costs lying between 20-25 million USD can be envisaged for equipment (highest cost for the compressor and for the ethanol concentration column, besides the three reactor stages) and 7.7-9.3 million USD per year for utilities, in which the highest cost is for steam.

The other important operating cost is ethanol itself, which has for sure an unsustainable impact if anhydrous from second generation biomass but also possibly form first generation, as determined for other related processes such as centralized hydrogen production [70] or ethylene synthesis [71]. Both processes were indeed OpEx intensive, with a determinant role of the cost of bioethanol for the economic sustainability of the solution. We expect similar outcome here.

From this point of view we should also consider that the bioethanol rectification form the raw beer (even very diluted, down to 3.5 mol%) is accomplished in this process using the ethylene glycol internally produced to resolve the water-ethanol azoetrope. This column has been designed as constituted of 7 Koch-Glitsch Superflux® valve trays followed by 5 m Koch-Glitsch Flexipac®HC® packings. The duty at the reboiler is significant, ca. 11.5 MW for the most diluted beer, constituting an important expenditure.

Conclusions

A full flowsheet for the direct one-pot conversion of bioethanol to ethylene oxide has been designed for the very first time. Such plant design is capable of converting more than 99% of the starting

ethanol into ethylene oxide into the once-through reactive section, with a selectivity around 84%. The overall yield is limited by the ethanol lost in the beer concentration and stripping operation, but this is a minor issue due to the relatively low cost of the reactant.

The separation section can recover ca. 98% of ethylene oxide produced in the reactive section, 90% as pure ethylene oxide and 8% as pure ethylene glycol. This products recovery section has been also effectively integrated with the raw materials purification line connecting the following steps: a) the concentrated ethanol is split between the reactor feed and the EO absorber, b) the EO left after its distillation is converted into glycol, c) part of the glycol is re-routed to the ethanol concentrator.

With the Pinch Analysis method, the heat consumption achieved after optimization was just 5.5 % higher with respect to the theoretical hot and cold utilities targets. A global $\Delta \boldsymbol{T_{min}}$ as low as 7 °C can be actually achieved considering the substantial contribution of latent heat exchanges.

Future works to improve the feasibility of the flowsheet design may focus on the following aspects: a more robust kinetic model, based on a higher number of experimental data, with deeper products analytical detail; addition of the treatment facilities for the vent and wastewater streams and wastewater treatment; evaluation of the hot and cold utilities kind and placement. Last but not least, this work is the fundamental basis to open the economic and the life-cycle assessments of the process.

List of acronyms

AcH	Acetaldehyde	**PA**	Pinch Analysis
EO	Ethylene Oxide	**PFR**	Plug-Flow reactor
EG	Ethylene Glycol	**VLE**	Vapor-Liquid Equilibrium
GCC	Grand Composite Curve		

List of symbols

A	(m^2)	area	$\mathcal{A}$		Anderson number
Cp	(kJ/kg°C)	heat capacity	$\mathcal{D}_{12}$	(m^2/s)	binary diffusion coefficient

Dp	(mm)	particle diameter	$\mathcal{D}_{mass}$	(m^2/s)	corrected binary diffusion coeff.
Ea	(kJ/kmol)	activation energy	$\mathcal{D}_K$	(m^2/s)	Knudsen diffusion coefficient
F	(kg/h)	mass flow	$\mathcal{D}_{eff}$	(m^2/s)	effective diffusion coefficient
h	(W/m^2K)	convective heat-exchange coeff.	α		stoichiometric coefficient
H	(kJ/kmol)	specific enthalpy	β		catalyst thermal number
HTU	(m)	packing unit height	ε	(m^3/m^3)	bed void fraction
k	(kmol/kg×s)	kinetic constant	η		catalyst efficiency
k_c	(W/mK)	thermal conductivity	θ	(m^3/m^3)	catalyst porosity
l		experiments index	ϑ	(m/m)	catalyst tortuosity
L	(m)	length	λ	(kg/m)	bed linear density
m	(mol/mol)	equilibrium ratio	μ	(Pa×s)	viscosity
n		moles number	ν		reaction order
N		packing units number	ρ	(kg/m^3)	density
NT		tube number	ρ_{mol}	(kmol/m^3)	molar density
OD, ID	(mm)	tube diameters	τ	(s)	contact time
P	(bar)	pressure	Φ		Thiele modulus
Q	(kW)	heat power			
r	(kmol/kg×s)	reaction rate			
R	(J/mol×K)	gas constant			
Re		Reynolds number			
T	(K)	temperature			
u	(m/s)	spatial velocity			
U	(W/m^2K)	overall heat-exchange coeff.			
V	(m^3)	volume			
w	(kg)	catalyst mass			
y	(mol/mol)	vapor fraction			
z	(m)	axial coordinate			

References

[1] Ethylene Oxide, Am. Chem. Soc. (2019).

[2] G.C.C. Mendes, T.R.S. Brandão, C.L.M. Silva, Ethylene oxide sterilization of medical devices: A review, Am. J. Infect. Control. 35 (2007) 574–581. doi:10.1016/j.ajic.2006.10.014.

[3] B. Evans, S. Hawkins, G. Schulz ed., Ullmann's Encyclopedy of Industrial Chemistry, VCH, Weinheim, 1991.

[4] International Agency for Research in Cancer, Ethylene Oxide, IARC Monogr. Eval. Carcinog. Risks To Humans. 97 (2008).

[5] T. Pu, H. Tian, M.E. Ford, S. Rangarajan, I.E. Wachs, Overview of Selective Oxidation of Ethylene to Ethylene Oxide by Ag Catalysts, ACS Catal. (2019) 10727–10750. doi:10.1021/acscatal.9b03443.

[6] S.A. Miller, Ethylene and Its Industrial Derivatives, Ernst Benn Ltd, London, 1969.

[7] A.N.R. Bos, L.A. Chewter, J.M. Kobe, Reactor System and Process for the Manufacture of Ethylene Oxide, US20090234144A1, 2009.

[8] Han van Milligen, Shell Global Solutions ENHANCEMENTS IN ETHYLENE OXIDE/ETHYLENE GLYCOL MANUFACTURING TECHNOLOGY, (2016).

[9] B.J. Ozero, J. V. Procelli, Can developments keep ethylene oxide viable, Hydrocarb. Process. 63 (1984).

[10] Z. Nawaz, Heterogeneous Reactor Modeling of an Industrial Multitubular Packed-Bed Ethylene Oxide Reactor, Chem. Eng. Technol. 39 (2016) 1845–1857. doi:10.1002/ceat.201500603.

[11] I.S. Yakovleva, S.P. Banzaraktsaeva, E. V. Ovchinnikova, V.A. Chumachenko, L.A. Isupova, Catalytic Dehydration of Bioethanol to Ethylene. Review, Katal. v Promyshlennosti. 16 (2016) 57–73. doi:10.18412/1816-0387-2016-1-57-73.

[12] P. Vondrová, Z. Tišler, J. Kocík, H. de Paz Carmona, M. Murat, Comparison of doped ZSM-5 and ferrierite catalysts in the dehydration of bioethanol to ethylene in a flow reactor, React. Kinet. Mech. Catal. 132 (2021) 449–462. doi:10.1007/s11144-021-01925-w.

[13] G. Chen, S. Li, F. Jiao, Q. Yuan, Catalytic dehydration of bioethanol to ethylene over TiO2/γ-Al2O3 catalysts in microchannel reactors, Catal. Today. 125 (2007) 111–119. doi:10.1016/j.cattod.2007.01.071.

[14] A. Tripodi, M. Belotti, I. Rossetti, Bioethylene Production: From Reaction Kinetics to Plant Design, ACS Sustain. Chem. Eng. 7 (2019) 13333–13350. doi:10.1021/acssuschemeng.9b02579.

[15] I. Rossetti, A. Tripodi, E. Bahadori, G. Ramis, Exploiting diluted bioethanol solutions for the production of ethylene: Preliminary process design and heat integration, Chem. Eng. Trans. 65 (2018). doi:10.3303/CET1865013.

[16] I. Rossetti, M. Compagnoni, G. De Guido, L.A. Pellegrini, G. Ramis, S. Dzwigaj, Ethylene production from diluted bioethanol solutions, Can. J. Chem. Eng. 95 (2017) 1752–1759.

doi:10.1002/cjce.22828.

[17] I. Rossetti, M. Compagnoni, E. Finocchio, G. Ramis, A. Di Michele, Y. Millot, et al., Ethylene production via catalytic dehydration of diluted bioethanol: a step towards an integrated biorefinery, Appl. Catal. B Environ. 210 (2017) 407–420.

[18] G. Pampararo, G. Garbarino, P. Riani, M. Villa García, V. Sánchez Escribano, G. Busca, A study of ethanol dehydrogenation to acetaldehyde over supported copper catalysts: Catalytic activity, deactivation and regeneration, Appl. Catal. A Gen. 602 (2020) 117710. doi:10.1016/j.apcata.2020.117710.

[19] P.I. Kyriienko, O. V. Larina, S.O. Soloviev, S.M. Orlyk, Catalytic Conversion of Ethanol Into 1,3-Butadiene: Achievements and Prospects: A Review, Theor. Exp. Chem. 56 (2020) 213–242. doi:10.1007/s11237-020-09654-2.

[20] C. Liu, Y. Li, L. Wu, Z. Geng, Synthesis of 1,3-butadiene from ethanol/acetaldehyde over ZrO2-MgO-SiO2 catalyst: The thermodynamics and reaction kinetics analysis, Chem. Eng. J. (2020) 127861. doi:10.1016/j.cej.2020.127861.

[21] I. Rossetti, A. Tripodi, G. Ramis, Hydrogen, ethylene and power production from bioethanol: Ready for the renewable market?, Int. J. Hydrogen Energy. 45 (2020). doi:10.1016/j.ijhydene.2019.07.201.

[22] I. Rossetti, M. Compagnoni, M. Torli, Process simulation and optimisation of H2 production from ethanol steam reforming and its use in fuel cells. 1. Thermodynamic and kinetic analysis, Chem. Eng. J. 281 (2015) 1024–1035. doi:10.1016/j.cej.2015.08.025.

[23] I. Rossetti, M. Compagnoni, M. Torli, Process simulation and optimization of H 2 production from ethanol steam reforming and its use in fuel cells . 2 . Process analysis and optimization, Chem. Eng. J. 281 (2015) 1036–1044. doi:10.1016/j.cej.2015.08.045.

[24] M. Compagnoni, A. Tripodi, I. Rossetti, Parametric study and kinetic testing for ethanol steam reforming, Appl. Catal. B Environ. 203 (2016) 899–909. doi:10.1016/j.apcatb.2016.11.002.

[25] A.R.T. Adriano H. Braga, Daniela C. de Oliveira, J.B.O. Santos, J.M.C.B. Jean Marcel R.

Gallo, Steam Reforming of Ethanol Using Ni–Co Catalysts Supported on MgAl2O4: Structural Study and Catalytic Properties at Different Temperatures, ACS Catal. 11 (2021) 2047–2061. doi:10.1021/acscatal.0c03351.

[26] X. Zhourong, W. Chan, W. Li, X. Jisheng, Z. Qiancheng, P. Lun, et al., Boosting hydrogen production from steam reforming of ethanol on nickel by lanthanum doped ceria, Appl. Catal. B Environ. 286 (2021). doi:10.1016/j.apcatb.2021.119884.

[27] W.-H. Chen, L. ShuCheng, L. Steven, C. Zih-Yu, J. Joon CHing, Reaction and hydrogen production phenomena of ethanol steam reforming in a catalytic membrane reactor, Energy. 220 (2020). doi:10.1016/j.energy.2020.119737.

[28] F. Folco, J.V. Ochoa, F. Cavani, L. Ott, M. Janssen, Ethanol gas-phase ammoxidation to acetonitrile, Catal. Sci. Technol. 7 (2017) 200–212. doi:10.1039/C6CY01275B.

[29] A. Tripodi, D. Ripamonti, R. Martinazzo, F. Folco, T. Tabanelli, F. Cavani, et al., Kinetic model for the ammoxidation of ethanol to acetonitrile, Chem. Eng. Sci. 207 (2019). doi:10.1016/j.ces.2019.07.015.

[30] A. Tripodi, E. Bahadori, D. Cespi, F. Passarini, F. Cavani, T. Tabanelli, et al., Acetonitrile from Bioethanol Ammoxidation: Process Design from the Grass-Roots and Life Cycle Analysis, ACS Sustain. Chem. Eng. 6 (2018) 5441–5451. doi:10.1021/acssuschemeng.8b00215.

[31] Renewable Ethylene, Ethylene Oxide & Ethylene Glycol, Sci. Des. Co. (n.d.).

[32] Z. Read, Croda Completes Ethanol to EO Plant in Delaware, Everchem Spec. Chem. (2017).

[33] M.J. Lippits, B.E. Nieuwenhuys, Direct conversion of ethanol into ethylene oxide on copper and silver nanoparticles: Effect of addition of CeOx and Li2O, Catal. Today. 154 (2010) 127–132. doi:10.1016/j.cattod.2010.03.019.

[34] M.J. Lippits, B.E. Nieuwenhuys, Direct conversion of ethanol into ethylene oxide on gold-based catalysts: Effect of CeOx and Li2O addition on the selectivity, J. Catal. 274 (2010) 142–149. doi:10.1016/j.jcat.2010.06.011.

[35] T.L. Silbaugh, P. Devlaminck, J.A. Sofranko, M.A. Barteau, Selective oxidation of ethanol over Ag, Cu and Au nanoparticles supported on Li2O/Γ-Al2O3, J. Catal. 364 (2018) 40–47. doi:10.1016/j.jcat.2018.05.011.

[36] P.D. Klugherz, P. Harriott, Kinetics of Ethylene Oxidation on a Supported Silver Catalyst, Am. Inst. Chem. Eng. 17 (1971) 856–866.

[37] R.A. Van Santen, H.P.C.E. Kuipers, The Mechanism of Ethylene Epoxidation, Adv. Catal. 35 (1987) 265–321. doi:10.1016/S0360-0564(08)60095-4.

[38] E.P.S. Schouten, P.C. Borman, K.R. Westerterp, Determination of the kinetics of ethene epoxidation, Chem. Eng. Process. Process Intensif. 35 (1996) 43–55. doi:10.1016/0255-2701(95)04109-5.

[39] E.P.S. Schouten, P.C. Borman, K.R. Westerterp, Influence of reaction products on the selective oxidation of ethene, Chem. Eng. Process. Process Intensif. 35 (1996) 107–120. doi:10.1016/0255-2701(95)04117-6.

[40] R.E. Kenson, M. Lapkin, Kinetics and mechanism of ethylene oxidation. Reactions of ethylene and ethylene oxide on a silver catalyst, J. Phys. Chem. 74 (1970) 1493–1502. doi:10.1021/j100702a017.

[41] G. Garbarino, R. Prasath Parameswari Vijayakumar, P. Riani, E. Finocchio, G. Busca, Ethanol and diethyl ether catalytic conversion over commercial alumina and lanthanum-doped alumina: Reaction paths, catalyst structure and coking, Appl. Catal. B Environ. 236 (2018) 490–500. doi:10.1016/j.apcatb.2018.05.039.

[42] J.F. DeWilde, H. Chiang, D.A. Hickman, C.R. Ho, A. Bhan, Kinetics and mechanism of ethanol dehydration on Al 2O3: The critical role of dimer inhibition, ACS Catal. 3 (2013) 798–807. doi:10.1021/cs400051k.

[43] C.X. Martins, C.J.A. Mota, Studies on direct conversion of ethanol into ethylene oxide on zeolites, Rev. Virtual Quim. 6 (2014) 1282–1294. doi:10.5935/1984-6835.20140084.

[44] A. Tripodi, M. Compagnoni, I. Rossetti, Kinetic modeling and reactor simulation for ethanol

steam reforming, ChemCatChem. 8 (2016) 3804 – 3813. doi:10.1002/cctc.201601075.

[45] L. Chi-Hsiung, B.A. Finlayson, Heat Transfer in Packed Beds-a reevalution, Chem. Eng. Sci. 32 (1977).

[46] G.A. Melhem, A. Gianetto, M.E. Levin, H.G. Fisher, S. Chippett, S.K. Singh, et al., Kinetics of the reactions of ethylene oxide with water and ethylene glycols, Process Saf. Prog. 20 (2001) 231–246. doi:10.1002/prs.680200405.

[47] J.W. van Hal, J.S. Ledford, X. Zhang, Investigation of three types of catalysts for the hydration of ethylene oxide (EO) to monoethylene glycol (MEG), Catal. Today. 123 (2007) 310–315. doi:10.1016/j.cattod.2007.02.015.

[48] J. Pla-Franco, E. Lladosa, S. Loras, J.B. Montón, Phase equilibria for the ternary systems ethanol, water+ethylene glycol or + glycerol at 101.3kPa, Fluid Phase Equilib. 341 (2013) 54–60. doi:10.1016/j.fluid.2012.12.022.

[49] C.F. Bonilla, S. Baron, Absorption of ethylene oxide in a Packed Column with Various Solvents, AIChE J. 1 (1955) 49–54.

[50] K.F. Coles, F. Popper, Vapor-Liquid Equilibria. Ethylene Oxide - Acetaldehyde and Ethylene Oxide - Water Systems, Ind. Eng. Chem. 42 (1950) 1434–1438. doi:10.1021/ie50487a046.

[51] Y.L. Huang, T. Merker, M. Heilig, H. Hasse, J. Vrabec, Molecular modeling and simulation of vapor-liquid equilibria of ethylene oxide, ethylene glycol, and water as well as their binary mixtures, Ind. Eng. Chem. Res. 51 (2012) 7428–7440. doi:10.1021/ie300248z.

[52] N. Kamihama, H. Matsuda, K. Kurihara, K. Tochigi, S. Oba, Isobaric vapor-liquid equilibria for ethanol + water + ethylene glycol and its constituent three binary systems, J. Chem. Eng. Data. 57 (2012) 339–344. doi:10.1021/je2008704.

[53] V. Bareggi, S. Mori, P. Schwarz, P. Beltrame, Equilibrio liquido-vapore del sistema acetaldeide-acqua sotto pressione, La Chim. e L'industria. 50 (1968) 1224–1226.

[54] L. Zhang, X. Wang, X. Zhu, D. Shen, Experimental Measurement and Modeling of Vapor–Liquid Equilibrium for the Ternary Systems Water + Ethanol + Ethylene Glycol, Water + 2-

Propanol + Ethylene Glycol, and Water + 1-Propanol + Ethylene Glycol, J. Chem. Eng. Data. 61 (2016) 2596–2604. doi:10.1021/acs.jced.6b00264.

[55] J.V. Rojas, L. Stinguel, M.R. Wolf-Maciel, R. Guirardello, Modeling and simulating complete extractive distillation process of ethanol-water mixture using equilibrium-stage distillation model and efficiency correlations (Barros & Wolf) on EMSO platform, Chem. Eng. Trans. 50 (2016) 331–336. doi:10.3303/CET1650056.

[56] S. Zaboon, A. Soames, V. Ghodkay, R. Gubner, A. Barifcani, Recovery of mono-ethylene glycol by distillation and the impact of dissolved salts evaluated through simulation of field data, J. Nat. Gas Sci. Eng. 44 (2017) 214–232. doi:10.1016/j.jngse.2017.04.007.

[57] A.H. Beebe, K.E. Coulter, R.A. Lindsay, E.M. Baker, Equilibria in Ethanol-Water System at Pressures Less Than Atmospheric, Ind. Eng. Chem. 34 (1942) 1501–1504. doi:10.1021/ie50396a019.

[58] R. Taylor, R. Krishna, Multicomponent Mass Transfer, Wiley, New York, 1193.

[59] B.D. Smith, Design of Equilibrium Stage Processes, McGraw-Hill, New York, 1963.

[60] D.W. Green, R.H. Perry, Perry's Chemical Engineers' Handbook, 8th ed., The McGraw-Hill Companies, Inc, 2008.

[61] F. Delannoy, G. Letray, Process for separating ethylene oxide from aldehyde impurities by distillation, US Patent 4966657, 1990.

[62] T. Gamse, Hydrodynamic Layout of Columns, Graz University of Technology, n.d.

[63] S. Karatzos, J. Mcmillan, J. Saddler, The potential and challenges of "drop in" biofuels, 2014.

[64] D.R. Summers, Rectifier design for fuel ethanol plants, in: Adv. Distill. Equip. Appl. Pap. 264b, San Francisco, CA, 2006.

[65] B. Bessling, S. Zeck, J. Pliickhan, T. Mayer, U. Loffler, G. Spiegel, et al., PROCESS FOR DISTILLING ETHYLENE OXIDE, 6123812, 2000.

[66] C. Madeddu, E. Massimiliano, R. Baratti, CO2 Capture by Reactive Absorption-Stripping, Springer, 2019.

[67] I.C. Kemp, Pinch analysis and process integration: A user guide on process integration for the efficient use of energy, 2nd ed., Butterworth-Heinemann, an imprint of Elsevier, Linacre House, Jordan Hill, Oxford OX2 8DP, UK 30, 2007. doi:http://dx.doi.org/10.1016/B978-075068260-2.50003-1.

[68] M.R. Altiokka, S. Akyalçin, Kinetics of the hydration of ethylene oxide in the presence of heterogeneous catalyst, Ind. Eng. Chem. Res. 48 (2009) 10840–10844. doi:10.1021/ie901037w.

[69] Koch-Glitsch, Fouling Services Trays - SUPERFLUX® Tray, (n.d.).

[70] M. Compagnoni, E. Mostafavi, A. Tripodi, N. Mahinpey, I. Rossetti, Techno-economic analysis of a bioethanol to hydrogen centralized plant, Energy&Fuels. 31 (2017) 12988–12996. doi:10.1021/acs.energyfuels.7b02434.

[71] M. Frosi, A. Tripodi, F. Conte, G. Ramis, N. Mahinpey, I. Rossetti, Ethylene from renewable ethanol: Process optimisation and economic feasibility assessment, J. Ind. Eng. Chem. (n.d.).